NASA Technical Memorandum 2002–206892, Volume 16

SeaWiFS Postlaunch Technical Report Series

Stanford B. Hooker, Editor
NASA Goddard Space Flight Center
Greenbelt, Maryland

Elaine R. Firestone, Senior Scientific Technical Editor
Science Applications International Corporation
Beltsville, Maryland

Volume 16, Navigation Algorithms for the SeaWiFS Mission

Frederick S. Patt
Science Applications International Corporation
Beltsville, Maryland

Abstract

The navigation algorithms for the Sea-viewing Wide Field-of-view Sensor (SeaWiFS were designed to meet the requirement of 1-pixel accuracy—a standard deviation (σ) of 2. The objective has been to extract the best possible accuracy from the spacecraft telemetry and avoid the need for costly manual renavigation or geometric rectification. The requirement is addressed by postprocessing of both the Global Positioning System (GPS) receiver and Attitude Control System (ACS) data in the spacecraft telemetry stream. The navigation algorithms described are separated into four areas: orbit processing, attitude sensor processing, attitude determination, and final navigation processing. There has been substantial modification during the mission of the attitude determination and attitude sensor processing algorithms. For the former, the basic approach was completely changed during the first year of the mission, from a single-frame deterministic method to a Kalman smoother. This was done for several reasons: a) to improve the overall accuracy of the attitude determination, particularly near the sub-solar point; b) to reduce discontinuities; c) to support the single-ACS-string spacecraft operation that was started after the first mission year, which causes gaps in attitude sensor coverage; and d) to handle data quality problems (which became evident after launch) in the direct-broadcast data. The changes to the attitude sensor processing algorithms primarily involved the development of a model for the Earth horizon height, also needed for single-string operation; the incorporation of improved sensor calibration data; and improved data quality checking and smoothing to handle the data quality issues. The attitude sensor alignments have also been revised multiple times, generally in conjunction with the other changes. The orbit and final navigation processing algorithms have remained largely unchanged during the mission, aside from refinements to data quality checking. Although further improvements are certainly possible, future evolution of the algorithms is expected to be limited to refinements of the methods presented here, and no substantial changes are anticipated.

1. INTRODUCTION

The navigation processing for the Sea-viewing Wide Field-of-view Sensor (SeaWiFS) data is performed as part of the level-0 to -1a conversion. The level-0 to -1a software extracts and converts the required telemetry from the data stream and passes it to the navigation code, which produces per-scan-line spacecraft position and instrument pointing information. The output of navigation is stored in the level-1a data products for use by downstream processing.

The navigation code is composed of two, largely independent subsystems: orbit processing, which filters the data from the onboard global positioning system (GPS) receiver to produce orbit vectors; and attitude processing, which filters the spacecraft attitude control system (ACS) telemetry and instrument tilt telemetry to determine the SeaWiFS sensor orientation.

The remainder of this section defines constants, reference frames, and transformations which are used in the algorithm descriptions.

1.1 Constants

The following constants are defined here for later use:

- R_E, Earth equatorial radius (6,378.137 km);
- R_M, Earth mean radius (6,371 km);
- f, dimensionless Earth flattening factor (1/298.257);
- ω_E, Earth rotation rate ($7.29211585494\times10^{-5}\,\mathrm{s}^{-1}$);
- ω_O, nominal Orbit angular rate ($2\pi/5940$);
- G_m, Earth gravitational constant ($398600.5\,\mathrm{km}^3\,\mathrm{s}^{-2}$); and
- J_2, dimensionless Earth gravity field perturbation term (1.08263×10^{-3}).

1.2 Reference Frames

In order to describe the navigation algorithms, several basic reference frames (all frames have orthonormal axes) are defined below.

a. *Earth-Centered Inertial (ECI):* This reference frame has its origin at the Earth's center and is inertially fixed. The axes are defined as: x on the equator at the vernal equinox; z at the North Pole; y orthogonal to z and x in the right-hand sense.

b. *Earth-Centered Earth-Fixed (ECEF):* This reference frame also has its origin at the Earth's center and rotates with the Earth. The axes are defined as: x at 0° latitude and longitude (Greenwich meridian at the equator); y at 0° latitude and 90° longitude; and z at the North Pole (also known as Earth-Centered Rotating, or ECR).

c. *Orbital:* This frame has its origin at the spacecraft position and is defined as: x-axis along the geodetic nadir vector; y-axis perpendicular to x and opposite the spacecraft velocity vector; and z-axis toward the orbit normal.

d. *Spacecraft:* This frame has its origin at the spacecraft position and is defined in the same sense as the orbital frame; during normal spacecraft operations the two are related by a small rotation which is specified by a pitch (θ), roll (ϕ), and yaw (ψ) Euler angle sequence.

e. *SeaWiFS Base:* This frame is nearly the same as the spacecraft frame except for a small, constant misalignment transformation.

f. *SeaWiFS Instrument:* This frame is related to the SeaWiFS base frame by the tilt angle, i.e., a rotation about the z-axis, which is common to both frames.

1.3 Transformations

The transformations among the ECI, ECEF, orbital, and spacecraft reference frames defined above are described in the following sections.

1.3.1 ECI-to-ECEF Transformation

The ECI-to-ECEF transformation consists of a rotation of the Greenwich hour angle (ξ) about the z-axis (Patt and Gregg 1994):

$$\mathbb{E} = \begin{bmatrix} \cos\xi & \sin\xi & 0 \\ -\sin\xi & \cos\xi & 0 \\ 0 & 0 & 1 \end{bmatrix}. \quad (1)$$

1.3.2 ECEF-to-Orbital Transformation

The ECEF-to-orbital transformation is derived from the orbit position and velocity vectors, $\vec{P}$ and $\vec{V}$, in the ECEF frame (Patt and Gregg 1994). First, the nadir vector at the spacecraft position is calculated. This is not a closed-form calculation, but a very good approximation is given by (Patt and Gregg 1994):

$$\vec{O}_x = -\begin{bmatrix} (1-f_P)^2 P_x \\ (1-f_P)^2 P_y \\ P_z \end{bmatrix} \frac{1}{\sqrt{P_z^2 + (1-f_P)^4 (P_x^2 + P_y^2)}}, \quad (2)$$

where $\vec{O}_x$ is the geodetic nadir vector, and f_P is the effective flattening factor at the spacecraft position. The latter is computed as follows:

$$(1-f_P)^2 = \frac{R_M(1-f)^2 + |\vec{P}| - R_M}{|\vec{P}|}, \quad (3)$$

where R_M is the Earth mean radius. The remaining axes of the orbital frame are defined as:

$$\vec{O}_z = \frac{\vec{V}_C \times \vec{O}_x}{|\vec{V}_C \times \vec{O}_x|}, \quad (4)$$

and

$$\vec{O}_y = \vec{O}_z \times \vec{O}_x, \quad (5)$$

where $\vec{V}_C$ is the orbit velocity vector corrected for the Earth's rotation rate,

$$\vec{V}_C = \begin{bmatrix} V_x - \omega_E V_y \\ V_y + \omega_E V_x \\ V_z \end{bmatrix}. \quad (6)$$

The full transformation is given by

$$\mathbb{O} = \begin{bmatrix} \vec{O}_x^T \\ \vec{O}_y^T \\ \vec{O}_z^T \end{bmatrix}. \quad (7)$$

where $\mathbb{O}$ is the ECEF-to-orbital transformation matrix.

1.3.3 Orbital-to-Spacecraft Transformation

The orbital-to-spacecraft transformation is defined by an Euler angle sequence. The order of rotations is pitch, roll, and yaw, which corresponds to z, y, and x in the spacecraft or orbital frame. The transformation is given by

$$\mathbb{B} = \mathbb{A}_\psi \mathbb{A}_\phi \mathbb{A}_\theta, \quad (8)$$

where

$$\mathbb{A}_\psi = \begin{bmatrix} 1 & 0 & 0 \\ 0 & \cos\psi & \sin\psi \\ 0 & -\sin\psi & \cos\psi \end{bmatrix}, \quad (9)$$

$$\mathbb{A}_\phi = \begin{bmatrix} \cos\phi & 0 & \sin\phi \\ 0 & 1 & 0 \\ -\sin\phi & 0 & \cos\phi \end{bmatrix}, \quad (10)$$

and

$$\mathbb{A}_\theta = \begin{bmatrix} \cos\theta & -\sin\theta & 0 \\ \sin\theta & \cos\theta & 0 \\ 0 & 0 & 1 \end{bmatrix}. \quad (11)$$

2. ORBIT PROCESSING

The orbit processing algorithms use the telemetry from the GPS receiver onboard OrbView-2† (OV2) to compute the spacecraft position at the time of each SeaWiFS scan line. The approach described here was designed to satisfy the following objectives: eliminate excursions and outliers in the data; and span intervals of missing, degraded, or corrupted data.

The approach is to use the GPS vectors from the telemetry as observations to be fit to a high-fidelity orbit model. The OV2 GPS receiver telemetry includes orbit position and velocity vectors in the ECEF frame, associated time tags, and the number of GPS satellites tracked. The telemetry is updated every 10 s.

† The spacecraft carrying the SeaWiFS instrument was originally named "SeaStar"; it was designated "OrbView-2" after launch.

The orbit model is based on the Artificial Satellite Analysis Program (ASAP), which was developed at the Jet Propulsion Laboratory (Kwok 1987) and is now available through the NASA Computer Software Management and Information Center (COSMIC) library of public domain software. ASAP is a Cowel orbit integration program which includes an Earth gravity model of up to 36 in degree and order, solar and lunar attractions, and atmospheric drag.

The processing for each interval is initialized using the results from the previous interval, which are saved as mean orbital elements at the ascending equator crossing. The orbit is integrated through the data interval using ASAP, and the vectors are extracted at the times of the GPS data samples. The position differences and partial derivatives, with respect to the initial elements, are computed and used to update the elements via a least-squares estimation. These calculations are iterated if necessary until the solution converges. The final elements are then used to integrate the orbit through the data interval, and the orbit vectors are interpolated to the SeaWiFS scan line times. The details of the orbit processing are presented in the following sections.

2.1 Orbit Integration and Interpolation

The ASAP orbit model and integration algorithm are described in Kwok (1987) and will not be repeated here. The model is initialized using mean elements, which consist of the semimajor axis (a), eccentricity (e), inclination (i), right ascension of the ascending node (l), argument of perigee (w), and mean anomaly (m). A 60 s output interval is selected. Additional force terms (e.g., atmospheric drag, other-body attractions) are based on input parameters and models.

The vectors are generated by ASAP in the ECI frame and are transformed to the ECEF frame using the ECI-to-ECEF transformation from Sect. 1.2. The vectors are interpolated to intermediate times using cubic interpolation, which combines the position and velocity of each component as the displacement and first derivative of a scalar function. If the time tags of two successive vectors are arbitrarily assigned values of 0 and 1, then the cubic polynomial coefficients are computed as follows:

$$\vec{c}_0 \;=\; \vec{P}_1, \tag{12}$$

$$\vec{c}_1 \;=\; \vec{V}_1 \Delta t, \tag{13}$$

$$\vec{c}_2 \;=\; 3\vec{P}_2 \;-\; 3\vec{P}_1 \;-\; 2\vec{V}_1\,\Delta t \;-\; \vec{V}_2 \Delta t, \tag{14}$$

and

$$\vec{c}_3 \;=\; 2\vec{P}_1 \;-\; 2\vec{P}_2 \;+\; \vec{V}_1 \Delta t \;+\; \vec{V}_2 \Delta t, \tag{15}$$

where $\vec{P}_1$ and $\vec{P}_2$ are the position vectors at times t_1 and t_2; $\vec{V}_1$ and $\vec{V}_2$ are the velocity vectors; $\Delta t = t_1 - t_2$ is the time difference (nominally 60 s); and $\vec{c}_0$, $\vec{c}_1$, $\vec{c}_2$, and $\vec{c}_3$ are the vectors of cubic polynomial coefficients. The vectors at intermediate times are then calculated as:

$$\vec{P} \;=\; \vec{c}_0 \;+\; \vec{c}_1 t \;+\; \vec{c}_2 t^2 \;+\; \vec{c}_3 t^3, \tag{16}$$

and

$$\vec{V} \;=\; \frac{\vec{c}_1 \;+\; 2\vec{c}_2 t \;+\; 3\vec{c}_3 t^2}{\Delta t}, \tag{17}$$

where $\vec{P}$ is the position vector at time t_S; similarly for $\vec{V}$; and $t = (t_S - t_1)/\Delta t$ is the relative time, for which t_S is the desired sample time. This algorithm is used for interpolating the vectors to both the GPS sample times and the SeaWiFS scan line times.

2.2 Partial Derivatives

The least-squares algorithm requires that partial derivatives of the orbit position components be computed at each data point with respect to changes in the initial mean elements. Calculation of analytic partial derivatives accounting for all force model terms would be complex. For small changes to the initial elements, however, most terms can be neglected, and good results are achieved by considering only the central body force and the J_2 (oblateness) term. The partial derivatives can be expressed in terms of the initial elements, the position and velocity vectors, and the elapsed time from the element epoch. The derivatives with respect to each element are computed as follows (note that in these equations all angles have units of radians).

2.2.1 Semimajor Axis

The partial derivatives with respect to the semimajor axis are computed as:

$$\frac{\partial \vec{P}}{\partial a} \;=\; \frac{\vec{P} \;-\; \frac{3}{2}(t \;-\; t_0)\vec{V}}{|\vec{P}|}, \tag{18}$$

where $\vec{P}$ is the orbit position vector, $\vec{V}$ is the orbit velocity vector, t is the time tag for the vector and t_0 is the initial element epoch.

2.2.2 Eccentricity

The partial derivatives with respect to the eccentricity are computed as:

$$\frac{\partial \vec{P}}{\partial e} \;=\; \frac{2|\vec{P}|\;\vec{V}\sin\nu}{|\vec{V}|} \;-\; \vec{P}\cos\nu, \tag{19}$$

where ν, the true anomaly, is computed as

$$\nu \;=\; o \;-\; w \;-\; (t - t_0)\,\frac{dw}{dt}. \tag{20}$$

The time of the orbit vector is t; t_0 is the epoch of the orbital elements; and o is the orbit angle measured from the ascending node:

$$o \;=\; \tan^{-1}\left\{\frac{P_z}{\sin(i)\big(P_x\cos(l) \;+\; P_y\sin(l)\big)}\right\}, \tag{21}$$

using the signs of the numerator and denominator to evaluate the arctangent over the range of $-\pi$ to π; and

$$\frac{dw}{dt} \;=\; \frac{3}{2}\,J_2\,\sqrt{G_m}\,R_E^2\,a^{-7/2}\Big(2 \;-\; \frac{5}{2}\sin^2(i)\Big), \qquad (22)$$

is the time derivative of the argument of perigee.

2.2.3 Right Ascension of the Ascending Node

The partial derivatives with respect to the right ascension of the ascending node are computed as:

$$\frac{\partial \vec{P}}{\partial l} \;=\; \vec{Z} \;\times\; \vec{P}, \qquad (23)$$

where $\vec{Z}$ is the geocentric North Pole vector $(0, 0, 1)^T$.

2.2.4 Argument of Perigee

The partial derivatives with respect to the argument of perigee are computed as:

$$\frac{\partial \vec{P}}{\partial w} \;=\; \vec{P}\sin\nu \;-\; e\frac{2|\vec{P}|\vec{V}\cos\nu}{|\vec{V}|}. \qquad (24)$$

Note that for near-circular orbits, the total effect of a change in the argument of perigee is nearly the same as for the mean anomaly, with the difference being a small periodic term. To avoid degeneracy, this equation includes only the periodic term, and the final value of the mean anomaly is corrected to account for the computed change in the argument of perigee.

2.2.5 Mean Anomaly

The partial derivatives with respect to the mean anomaly are computed as:

$$\frac{\partial \vec{P}}{\partial m} \;=\; \frac{\vec{V}}{n}\;(t \;-\; t_0), \qquad (25)$$

where

$$\begin{aligned} n =& \frac{dm}{dt} \\ =& \sqrt{\frac{G_m}{a^3}}\left\{1 + \frac{3}{2}\;J_2\left(\frac{R_E}{a}\right)^2\big(4\cos^2(i) - 1\big)\right\}, \end{aligned} \qquad (26)$$

is the mean motion.

2.2.6 Inclination

The partial derivatives with respect to the inclination are computed as:

$$\frac{\partial \vec{P}}{\partial i} \;=\; \vec{L}\sin(o) \;+\; \frac{\partial l}{\partial i}\;\frac{\partial \vec{P}}{\partial l} \;+\; \frac{\partial m}{\partial i}\;\frac{\partial \vec{P}}{\partial m}, \qquad (27)$$

where

$$\vec{L} \;=\; \frac{\vec{P}\times\vec{V}}{|\vec{P}\times\vec{V}|}, \qquad (28)$$

is the orbit plane normal vector;

$$\frac{\partial l}{\partial i} \;=\; \frac{3}{2}\;J_2\sqrt{G_m}R_E^2\;a^{-7/2}\;\sin(i)\;(t \;-\; t_0), \qquad (29)$$

is the derivative of the right ascension of the ascending node with respect to i; and

$$\frac{\partial m}{\partial i} \;=\; 12J_2\sqrt{G_m}R_E^2\;a^{-7/2}\;\sin(i)\;(t \;-\; t_0), \qquad (30)$$

is the derivative of the mean anomaly with respect to i.

These equations are complete as given; however, some computational efficiency is gained by taking advantage of relationships between orbital elements and the orbit vectors themselves, thereby reducing the number of trigonometric function evaluations. Specifically,

$$\sin(l) \;=\; \frac{L_x}{\sqrt{L_x^2 \;+\; L_y^2}}, \qquad (31)$$

$$\cos(l) \;=\; \frac{-L_y}{\sqrt{L_x^2 \;+\; L_y^2}}, \qquad (32)$$

$$\sin(i) \;=\; \sqrt{L_x^2 \;+\; L_y^2}, \qquad (33)$$

and

$$\cos(i) \;=\; L_z. \qquad (34)$$

2.3 Least-Squares Update Procedure

The initial orbital elements are updated to fit the GPS orbit position vectors using a batch-weighted, least-squares algorithm, based on the Gauss-Newton procedure (Fallon and Rigterink 1978). The 6-element state vector, $\vec{X}$, is the initial set of orbital elements; the measurement vector consists of the individual components of the GPS orbit position vectors, with each component treated as an independent measurement; and the observation model vector is the corresponding set of position components generated from the orbital elements.

The partial derivative matrix is generated using (18)–(34) for each orbit position vector, with the following additional calculations performed. First, the derivatives with respect to angles (i, l, w, and m) are scaled from radians to degrees, to be consistent with the units of the elements themselves. Second, the derivatives with respect to eccentricity are about two orders of magnitude larger, and those with respect to the argument of perigee are about the same factor smaller, than those with respect to the other elements; to avoid numerical errors in the calculations, these derivatives are scaled by factors of 0.01 and 100, respectively, with these scalings later removed from the updates.

Table 1. The conversion factors for attitude sensor measurements.

Sensor	*Scale Factor*	*Offset*	*Range*
Sun Sensor	2.0022498×10^{-4}	-2.050304	± 2.050304
Horizon Scanner	5.4931641×10^{-3}	0.0	0–360°

Prior to the actual fitting procedure, the input GPS vectors are validated. First, the total number of vectors is required to be above a specified minimum value; if fewer vectors are available, the initial elements are integrated through the data interval and used directly for navigation, with no update performed. Second, the number of GPS satellites tracked for each measured vector must be at least four, the minimum value required to obtain a valid GPS measurement. Third, the magnitude of the orbit position vector is required to be within a specified range. Finally, rejection of outliers is performed by computing the interquartile range (IQR) for the initial set of measurement residuals; any vectors with residuals greater than a specified multiple of the IQR are rejected.

The corrections to the state vector are computed as:

$$\Delta\vec{X} = [\mathbb{W} + \mathbb{G}^T\mathbb{G}]^{-1}[\mathbb{G}^T(\vec{Y} - \vec{G})], \qquad (35)$$

where $\Delta\vec{X}$ is the 6-element state update vector; $\mathbb{W}$ is the 6×6 state weight matrix; $\mathbb{G}$ is the matrix of partial derivatives of $\vec{G}$ with respect to $\vec{X}$; $\vec{Y}$ is the vector of GPS orbit position measurements; and $\vec{G}$ is the vector of corresponding orbit position components generated from the initial orbital elements. The state weights are chosen to avoid anomalous updates due to reduced visibility on some elements for short data intervals [i.e., high-resolution picture transmission (HRPT) scenes of 10–15 m], while allowing rapid convergence for longer intervals (onboard recorder downlinks of approximately 12 h). The measurement weights are implicitly set to unity.

Prior to their application, the updates to the eccentricity and the argument of perigee are scaled by the same factors as the associated derivatives (0.01 and 100, respectively); and the update for the argument of perigee is subtracted from that for the mean anomaly, as described above in the calculation of the derivative with respect to the argument of perigee.

The state vector updates are tested for convergence by comparing them with specified tolerances. The tolerances are chosen to represent a maximum position change of approximately 100 m over 12 h: 0.002 km for a; 0.00001 for e; 0.1 for w; and 0.001 for i, l, and m. If the update to any element exceeds the tolerance, the entire process (orbit integration and interpolation, partial derivative calculation and least-squares update) is iterated using the updated orbital elements.

2.4 Final Orbit Processing

The converged orbital elements are used to generate the orbit vectors for use in attitude processing and geolocation of the scan lines in the interval. The orbit is integrated through the data interval using the ASAP model and the converged elements, and orbit vectors are stored every 60 s. During attitude processing for individual scenes—global area coverage (GAC) orbits, local area coverage (LAC) segments, or HRPT scenes—the orbit is interpolated to the scan line times using (12)–(17).

The results of GPS orbit fitting are stored for use in future reprocessing, to avoid the need to repeat the fitting process, and to initialize the fitting process for the next data interval. This is performed by saving the mean elements at each ascending node crossing in a permanent disk file. The converged orbital elements at the start of the interval are saved, and the orbit vector at each node crossing (i.e., the first vector north of the equator in each orbit) is converted to mean elements, which are appended to the file. The algorithm for converting the orbit vectors to mean elements is included in the ASAP program.

3. ACS SENSOR PROCESSING

The OV2 attitude is computed using the spacecraft attitude sensor data, along with the orbit vectors produced by filtering the GPS data. The first step is filtering and converting the attitude sensor data. The OV2 attitude sensor complement consists of three two-axis digital sun sensors (DSS) and two horizon scanners (HS). The sample rate is once per 10 s in GAC data and once per 2 s in LAC and HRPT data. Note that because the ACS telemetry are included twice per second in LAC and HRPT data, the samples are repeated four times each. The conversions from digital telemetry to analog measurements for the sensors are given in Table 1. The processing converts each sensor output to unit vectors in the spacecraft reference frame. The output and processing for each sensor are described separately.

3.1 Sun Sensor Processing

The following sections describe the DSS, their output, and the sensor data processing.

3.1.1 Sensor Description

The OV2 DSSs each measure the sun's direction in two axes, with a field-of-view (FOV) of ±64° along each axis. The three sensors are mounted as follows: DSS-A is on the

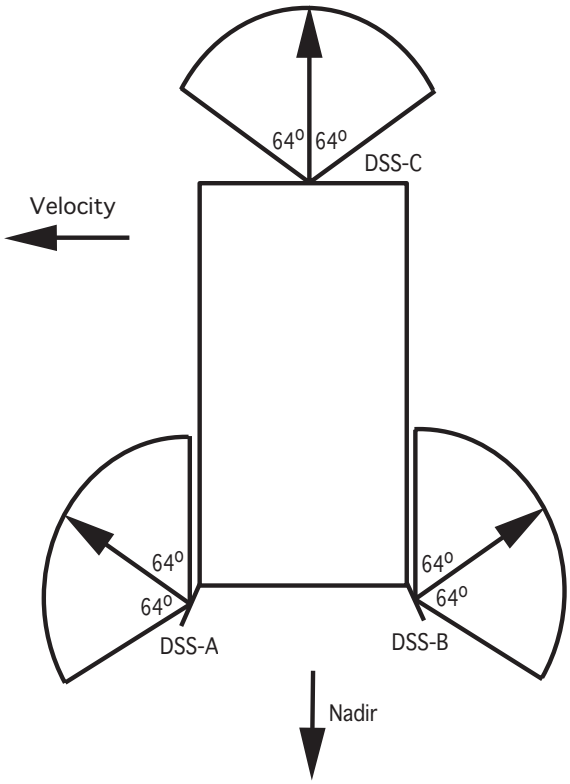

Fig. 1. The OrbView-2 digital sun sensor coverage.

forward side ($-y$ axis) of the spacecraft, with its boresight angled 26° upward (toward the $-x$ axis); DSS-B is on the rearward ($+y$) side, also with its boresight angled 26° upward; DSS-C is on the spacecraft top deck, with its boresight along the zenith ($-x$) direction. The DSSs, therefore, provide continuous and overlapping coverage during the orbit day. The coverage of the DSSs is illustrated in Fig. 1.

The output of each sun sensor are the tangents of the two projected angles (Chen and Lerner 1978), time tag, and status words. The tangents are digitized with a range of 0–20,479 counts and are converted to engineering units as given in Table 1. The time tags are given in milliseconds of the week, and are converted to a time offset from the minor frame time tag. The status words include the sun presence bit, which indicates whether the sun is within the sensor FOV.

3.1.2 Sensor Data Processing

The steps in the processing of the sun sensor data are: validation, smoothing and interpolation, transformation, and averaging. The first two steps are performed independently for each output of each DSS, the two output values for each DSS are combined during the transformation, and the final stage produces a single vector from all sensors.

The validation is performed in three steps. First, the valid arc for each sensor is determined as the interval during which the sun presence is indicated by the status word. Second, the data along each axis are limit-checked against an absolute range. Third, the consecutive samples for each axis are checked for consistency via a delta limit check. Samples which fail any test are rejected from further processing. The limits for the last two checks are adjustable parameters.

The smoothing and interpolation is performed as a single step, to reduce any remaining noise spikes and to interpolate the sensor samples to the SeaWiFS scan line times. This is performed using a moving-arc cubic polynomial. The polynomial is fit to a fixed number of samples, starting with the first valid sample, and evaluated at the scan line times. The sample range is then shifted by half of the number of samples, and the fitting-evaluation process is repeated. In the overlapping range, the final output is computed as a weighted average of the two polynomials, with the weight increasing linearly from the end to the center of the sample range for each fit. This process is repeated until the range of valid samples has been fitted.

The transformation converts the output of each DSS into unit vectors in the spacecraft frame. The output of the sensor is corrected using a linear scale factor and bias:

$$\tan\alpha' \;=\; A_\alpha \tan\alpha \;+\; B_\alpha, \tag{36}$$

and

$$\tan\beta' \;=\; A_\beta \tan\beta \;+\; B_\beta, \tag{37}$$

where $\tan\alpha$ and $\tan\beta$ are the sensor output values, which have been validated and smoothed; $\tan\alpha'$ and $\tan\beta'$ are

the calibrated values; A_α and A_β are the scale factors; and B_α and B_β are the biases for the two axes. The results are converted to unit vectors in the DSS frame as follows (Chen and Lerner 1978; note that here the sensor x-axis is the boresight):

$$\vec{S}_D = \begin{bmatrix} 1 \\ \tan\alpha' \\ \tan\beta' \end{bmatrix} \frac{1}{\sqrt{1+\tan^2\alpha'+\tan^2\beta'}}, \quad (38)$$

and then transformed to the spacecraft frame:

$$\vec{S}_S = \mathbb{C}\,\vec{S}_D, \quad (39)$$

where $\mathbb{C}$ is the DSS-to-spacecraft transformation matrix.

The final step is to compute the average observed sun vector. For each scan line which had sun presence for two DSSs, the weighted average of the vectors from the DSSs is computed. The weight for each DSS is unity at the center of the FOV and decreases linearly to zero at the edges, based on the assumption that each DSS is most accurate near the center of the FOV.

3.2 Horizon Scanner Processing

The following sections describe the HSs, their output, and the sensor data processing.

3.2.1 Sensor Description

The OV2 HSs measure the Earth's horizon height (or, more precisely, the height of the CO_2 layer in the atmosphere) in the scanner reference frame. Each scanner has an optical element which scans a conical path (with a half-cone angle of 45°) as the sensor rotates. The scanner determines the rotation angle at which the optical element crosses the horizon from space to Earth (*in-crossing*) and vice versa (*out-crossing*). The scanner determines the rotation angle between the two crossings (Earth width, or chord) and the mid-point relative to a zero-reference angle (phase). These measurements are used to determine the unit nadir vector in the spacecraft frame.

The two scanners are mounted on opposite sides of the spacecraft lower deck, with their rotation axes toward the $-z$ (HS-A) and $+z$ (HS-B) axes. The rotation axes are canted 5° toward the $+x$ (downward) axis. Each scanner rotates in the right-hand sense about its outward-pointing axis. The HS geometry is illustrated in Fig. 2.

Each scanner has a *blanking region*, which is a 90° range of rotation for which the sensor view is obscured by the mounting hardware. The zero-reference for the phase measurement is centered within the blanking region, so the effective range for horizon crossing measurements is from 45–315°. The OV2 scanners are mounted with the zero-reference rotated 45° from the spacecraft upward (x-axis), to enable the scanners to be used both at nadir pointing and with the spacecraft pitched 90° for orbit raising. The nominal values for the phase measurements are about 225° and 135° for HS-A and HS-B, respectively, and about 120° for the chord measurements for both scanners.

The output of each horizon scanner consists of the chord and phase angles, time tag, and status words. The angles are digitized with a range of 0–65,535 counts and are converted to engineering units as given in Table 1. The time tags are given in milliseconds of the week, and are converted to a time offset from the minor frame time tag.

3.2.2 Sensor Data Processing

The processing of the horizon scanner data is more complicated than that for the sun sensors. The reason is that the quantity being measured—the height of the CO_2 layer in the atmosphere—is dynamic and varies with orbit position, as well as having seasonal and unmodeled variations. The total variation from the average is of the order of tenths of a degree, which is significant compared to the SeaWiFS pixel angle (0.091°), and therefore, the triggering height model is critical to the overall accuracy of the calculation.

The initial processing of the scanner data is very similar to that for the sun sensors. In the CO_2 band (14–16 μm), the scanners can view the Earth for the entire orbit, so there is no need to determine the valid data arc. The individual measurements are checked using both absolute and delta limits, smoothed and interpolated to the scan line times, using the moving-arc cubic polynomial method.

The conversion of the angles to the geocentric nadir in the spacecraft reference frame involves several steps: converting angles to horizon crossing vectors; calculating the model horizon angles at the crossings; and solving for the nadir vector.

3.2.2.1 Horizon Vectors

The phase and chord measurements are converted to incrossing and outcrossing angles, as follows:

$$\Phi_I = \Phi_S - \frac{\Omega}{2}, \quad (40)$$

and

$$\Phi_O = \Phi_S + \frac{\Omega}{2}, \quad (41)$$

where Φ_S is the phase angle, Ω is the chord angle, and Φ_I and Φ_O are the incrossing and outcrossing angles, respectively, relative to the zero reference for the scanner.

The crossing angles are calibrated using a look-up table generated from calibration data provided by the sensor vendor. A unique calibration table is provided for each angle, with measured and actual angles tabulated at 0.5° intervals. The actual crossing angles are computed by interpolating from the table entries to the input angles. A sample calibration table is illustrated in Fig. 3, which shows the difference between the input and output angles versus input angle for the HS-A incrossing angle.

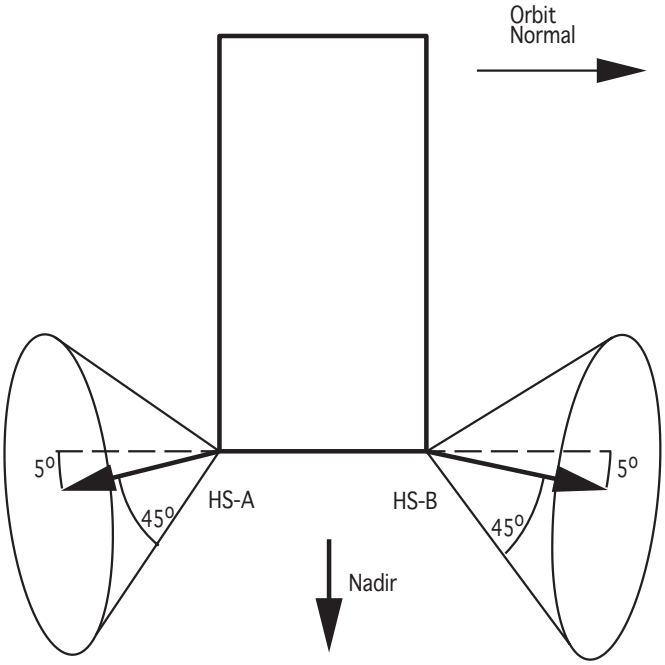

Fig. 2. The OrbView-2 horizon scanner geometry.

Each angle is then converted to a unit horizon crossing vector in the spacecraft frame:

$$\vec{H}_H \;=\; \begin{bmatrix} \cos\Phi\sin\gamma \\ \sin\Phi\sin\gamma \\ \cos\gamma \end{bmatrix}, \tag{42}$$

and

$$\vec{H}_S \;=\; |\mathbb{H}|\;\vec{H}_H, \tag{43}$$

where γ is the scanner half-cone angle of 45°, $\vec{H}_H$ is the horizon vector in the scanner reference frame, $\vec{H}_S$ is the vector in the spacecraft frame, and $\mathbb{H}$ is the scanner frame-to-spacecraft frame transformation matrix.

3.2.2.2 Horizon Angle Model

The model horizon height at each crossing is a function of several variables; the orbit geocentric latitude and position magnitude, the azimuth of the crossing point, and the height of the CO_2 layer (Liu 1978). Standard equations are available for computing the horizon angle based on static models; however, analysis of the OV2 horizon scanner data has shown that the apparent CO_2 height shifts seasonally (Patt and Bilanow 2001). The model described below was derived for SeaWiFS navigation in order to allow for this shift.

The horizon angle to the geocentric nadir, ρ, is computed by solving the following quadratic equation:

$$\begin{aligned} 0 = {} & H_4^2\cos^2\Psi \;-\; 4H_6\sin^2\Psi \;-\; 4H_1H_6\cos^2\Psi \\ & +\; (4H_3H_6\cos\Psi \;-\; 2H_4H_5\cos\Psi)\cot\rho \\ & +\; (H_5^2 \;-\; 4H_2H_6)\cot^2\rho\,, \end{aligned} \tag{44}$$

where Ψ is the azimuth of the horizon crossing relative to local north, and the coefficients H_1 through H_6 are computed as follows:

$$H_1 = \sin^2\lambda + \frac{\cos^2\lambda}{(1-f)^2}, \tag{45}$$

$$H_2 = \cos^2\lambda + \frac{\sin^2\lambda}{(1-f)^2}, \tag{46}$$

$$H_3 = -2\sin\lambda\cos\lambda + \frac{2\sin\lambda\cos\lambda}{(1-f)^2}, \tag{47}$$

$$H_4 = -2|\vec{P}|\sin\lambda\cos\lambda + \frac{2|\vec{P}|\sin\lambda\cos\lambda - 2\delta z\cos\lambda}{(1-f)^2}, \tag{48}$$

$$H_5 = 2|\vec{P}|\cos^2\lambda + \frac{2|\vec{P}|\sin^2\lambda - 2\delta z\sin\lambda}{(1-f)^2}, \tag{49}$$

and

$$H_6 = |\vec{P}|^2\cos^2\lambda + \frac{|\vec{P}|\sin\lambda - \delta z)^2}{(1-f)^2} - (R_E + \delta r)^2, \tag{50}$$

where λ is the orbit geocentric latitude, δz is a seasonal ellipsoid shift along the Earth's pole, and δr is a seasonal adjustment to the Earth's radius. The value of f for the Earth's surface is 1/298.257 (Wertz 1978); however, the flattening of the CO_2 layer is adjusted based on the analysis of the horizon scanner data (Patt and Bilanow 2001):

$$f \;=\; \frac{1}{185} \;-\; \frac{\sin\lambda_S}{640}, \tag{51}$$

where λ_S is the subsolar latitude for the sample time. The remaining seasonal corrections are computed as:

$$\delta z \;=\; 11\sin\lambda_S, \tag{52}$$

and

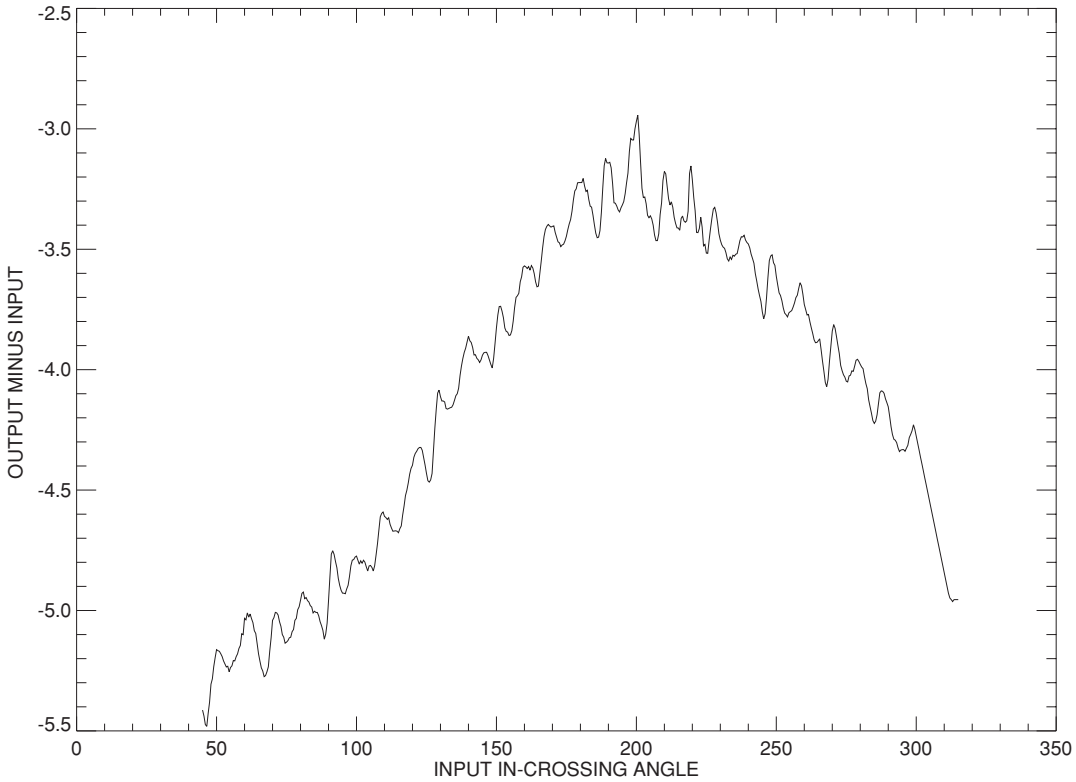

Fig. 3. The in-crossing angle calibration for HS-A, where the units are in degrees.

$$\delta r \;=\; -4.5 \sin \lambda_S. \tag{53}$$

The horizon crossing azimuth, Ψ, depends on the azimuth of the orbit reference frame y-axis, the spacecraft yaw angle, the scanner rotation axis in the spacecraft frame, and the Earth chord measurement. The orbital y-axis azimuth is determined relative to the local north direction at the orbit position, which is computed as

$$\vec{N} \;=\; \begin{bmatrix} -P_x P_z \\ -P_y P_z \\ P_x^2 + P_y^2 \end{bmatrix} \frac{1}{\sqrt{|\vec{P}|\;(P_x^2 + P_y^2)}}, \tag{54}$$

where $\vec{N}$ is the unit vector in the northern direction. The orbital azimuth given by

$$\Psi_O \;=\; -\tan^{-1}\left(\frac{\vec{N}\cdot\vec{O}_z}{\vec{N}\cdot\vec{O}_y}\right), \tag{55}$$

where Ψ_O is the azimuth of the orbital frame y-axis, and $\vec{O}_y$ and $\vec{O}_z$ are the orbital y- and z-axes, respectively. The spacecraft y-axis azimuth differs from the orbital azimuth by the yaw angle, and the scanner axis azimuths are $\pm 90°$ from the spacecraft, so the scanner axis azimuth is given by

$$\Psi_{HS} \;=\; \Psi_O + \psi - 90, \tag{56}$$

for HS-A and the same equation with $+90°$ is used for HS-B. The next step is to compute the azimuth offset from the scanner rotation axis to the horizon crossings. This offset is computed from the chord by first computing the horizon angle ρ_0 at the scanner axis azimuth using (45). Using this angle, the chord, and the scanner cone angle are used to compute the azimuth offset:

$$\Delta\Psi = \cos^{-1}\left\{\frac{\sin^2\gamma\cos\Omega + \cos^2\gamma - \cos^2\rho}{2\sin^2\rho}\right\}, \tag{57}$$

and

$$\Psi \;=\; \Psi_{HS} + \Delta\Psi, \tag{58}$$

where the offset is positive for the in-crossing and the same equation is used with a negative offset for the out-crossing.

The final step is to adjust ρ to account for the CO_2 layer height. This height is assumed to be 40 km, which is included by adding a bias of $0.74°$ to the value of ρ determined from (44).

Note that the spacecraft yaw angle is needed for (56). This would seem to be circular logic, because the nadir vector is ultimately used to compute yaw. The horizon angle, however, varies slowly with yaw (about 0.003), so the input to (56) need only be accurate to a few degrees. For the first scan, the yaw is assumed to be zero, and the calculations are repeated if the final yaw is larger than a specified tolerance. For all subsequent scans, the yaw is used from the previous scan.

3.2.2.3 Nadir Vector Calculation

The calculation of the nadir vector can be performed using data from either one or both scanners. If one scanner is used, the calculation is deterministic; for two scanners a least-squares estimation is performed. In either case the calculation is based on the following relationship between a horizon crossing vector, the corresponding horizon angle and the nadir vector:

$$\vec{H} \cdot \vec{E} \;=\; \cos\rho, \tag{59}$$

where $\vec{E}$ is the geocentric nadir vector in the spacecraft frame.

The deterministic calculation is performed by constructing a set of orthonormal axes using the two horizon crossing vectors, and then applying the above relationship to solve for $\vec{E}$. The axes are constructed as follows:

$$\vec{U}_1 \;=\; \frac{\vec{H}_1 \;+\; \vec{H}_2}{|\vec{H}_1 \;+\; \vec{H}_2|}, \tag{60}$$

$$\vec{U}_2 \;=\; \frac{\vec{H}_1 \times\; \vec{H}_2}{|\vec{H}_1 \times\; \vec{H}_2|}, \tag{61}$$

and

$$\vec{U}_3 \;=\; \frac{\vec{H}_1 \;-\; \vec{H}_2}{|\vec{H}_1 \;-\; \vec{H}_2|}. \tag{62}$$

Combining (60) and (62) with (59) above produces the following:

$$\begin{aligned} \vec{U}_1 \cdot \vec{E} \;&=\; \frac{\cos\rho_1 \;+\; \cos\rho_2}{|\vec{H}_1 \;+\; \vec{H}_2|} \\ &=\; u_1, \end{aligned} \tag{63}$$

and

$$\begin{aligned} \vec{U}_3 \cdot \vec{E} \;&=\; \frac{\cos\rho_1 \;-\; \cos\rho_2}{|\vec{H}_1 \;-\; \vec{H}_2|} \\ &=\; u_3. \end{aligned} \tag{64}$$

By definition, because $\vec{U}_1$, $\vec{U}_2$, and $\vec{U}_3$ are orthonormal,

$$\begin{aligned} \vec{U}_2 \cdot \vec{E} \;&=\; \sqrt{1 \;-\; u_1^2 \;-\; u_3^2} \\ &=\; u_2, \end{aligned} \tag{65}$$

and, therefore,

$$\vec{E} \;=\; u_1\vec{U}_1 \;+\; u_2\vec{U}_2 \;+\; u_3\vec{U}_3, \tag{66}$$

where u_1, u_2, and u_3, are intermediate coefficients used to calculate the nadir vector, and the sign of u_2, is chosen to ensure that the x component of the nadir vector is positive.

For more than two horizon crossing vectors (dual-scanner processing), the nadir vector is overdetermined, and a least-squares calculation is performed. The loss function is constructed from (59) as follows:

$$J \;=\; 0.5\sum_{i=1}^{4}\left[\vec{H}_i \cdot \vec{E} \;-\; \cos\rho_i\right]^2. \tag{67}$$

Minimizing (67) with respect to $\vec{E}$ yields:

$$\sum_{i=1}^{4}\vec{H}_i(\vec{H}_i \cdot \vec{E}) \;-\; \sum_{i=1}^{4}\vec{H}_i\cos\rho_i \;\equiv 0. \tag{68}$$

The formulation in (68) can be rearranged:

$$\left(\sum_{i=1}^{4}\vec{H}_i^T\vec{H}_i\right)\vec{E} \;=\; \sum_{i=1}^{4}\vec{H}_i\cos\rho_i, \tag{69}$$

which is solved for $\vec{E}$ by matrix inversion and multiplication. The final nadir vector is normalized to correct for any numerical errors.

4. ATTITUDE DETERMINATION

The attitude determination processing for SeaWiFS uses the computed sun and nadir vectors in the body frame, along with the reference sun and nadir vectors in the ECEF frame, to compute the yaw, roll, and pitch angles. A Kalman smoothing algorithm is used to reduce the uncertainty in the yaw angle near the subsolar point, allow processing through gaps in attitude sensor data, and minimize discontinuities caused by transitions in sensor coverage (i.e., DSS FOVs). The dynamics model is based on the assumption that the pitch axis is nearly inertial, which is due to the pitch momentum bias resulting from the momentum wheel.

The following sections present the equations used, followed by a description of the implementation.

4.1 Kalman Filter Equations

The basic Kalman filter equations are given (Fallon 1978) as follows. The state update equations are:

$$\vec{X}(t) \;=\; \vec{X}_{-1}(t) \;+\; \mathbb{K}(\vec{Y} \;-\; \vec{G}), \tag{70}$$

$$\mathbb{K} \;=\; \mathbb{P}_{-1}(t)\mathbb{G}^T\left[\mathbb{R} \;+\; \mathbb{G}\mathbb{P}_{-1}(t)\mathbb{G}^T\right]^{-1}, \tag{71}$$

and

$$\mathbb{P} \;=\; \left[\mathbb{I} - \mathbb{K}\mathbb{G}\right]\mathbb{P}_{-1}\left[\mathbb{I} - \mathbb{K}\mathbb{G}\right]^T \;+\; \mathbb{K}\mathbb{R}\mathbb{K}^T, \tag{72}$$

where $\vec{X}(t)$ is the state vector of dimension 3 at time t; $\vec{Y}$ is the observation vector of dimension 6; $\vec{G}$ is the observation model vector, also of dimension 6; $\mathbb{K}$ is the (3×6) gain matrix; $\mathbb{P}$ is the (3×3) state covariance matrix; $\mathbb{G}$ is the (6×3) matrix of partial derivatives of $\vec{G}$ with respect to $\vec{X}$; and $\mathbb{R}$ is the (6×6) observation covariance matrix. The subscript (-1) on $\vec{X}$ and $\mathbb{P}$ indicates a state at time t propagated from the previous time.

The state propagation equations are:

$$\vec{X}(t \;+\; \Delta t) \;=\; \mathbb{D}(t \;+\; \Delta t, t)\vec{X}(t), \tag{73}$$

and

$$\begin{aligned}\mathbb{P}(t\ +\ \Delta t)\ &= \mathbb{D}(t\ +\ \Delta t, t)\ \mathbb{P}(t)\ \mathbb{D}^T(t\ +\ \Delta t, t)\\ &+\ \mathbb{Q}(t\ +\ \Delta t, t),\end{aligned} \tag{74}$$

where $\mathbb{D}$ is the (3×3) state transition matrix, $\mathbb{Q}$ is the (3×3) state noise covariance matrix, and t is the time step.

For SeaWiFS attitude determination, the state $\vec{X}$ consists of the yaw, roll, and pitch attitude angles, and the observations $\vec{Y}$ consist of the components of the computed sun and nadir vectors. The calculations of $\vec{G}$, $\mathbb{G}$, $\mathbb{R}$, $\mathbb{Q}$, and $\mathbb{D}$ are performed as described in the remainder of this section.

The observation model is based on the reference sun and nadir vectors transformed to the spacecraft frame. The sun reference vector, $\vec{S}_E$, is computed in the ECEF frame from a model (Patt and Gregg 1994) and transformed from ECEF-to-spacecraft coordinates using the transformations given in Sect. 1.2:

$$\vec{S}_R\ =\ \mathbb{B}\,\mathbb{O}\,\vec{S}_E, \tag{75}$$

where $\vec{S}_R$ is the sun reference vector in the spacecraft frame; and $\mathbb{B}$ is computed using the propagated yaw, roll, and pitch. The reference nadir vector is the negative of the normalized orbit position vector, which is also transformed to spacecraft coordinates:

$$\vec{E}_R\ =\ \frac{-\mathbb{B}\mathbb{O}\vec{P}}{|\vec{P}|}, \tag{76}$$

and, therefore,

$$\vec{G}\ =\ \begin{bmatrix}\vec{S}_R\\ \vec{E}_R\end{bmatrix}. \tag{77}$$

The calculations for determining $\mathbb{G}$, the partial derivatives of these vectors with respect to $\vec{X}$, can be performed by recognizing that only the orbital-to-spacecraft transformation depends on $\vec{X}$; e.g.,

$$\frac{\partial S_R}{\partial \vec{X}}\ =\ \frac{\partial \mathbb{B}}{\partial \vec{X}}\ \mathbb{O}\vec{S}_E, \tag{78}$$

and likewise for $\vec{E}_R$. It is only necessary, therefore, to differentiate the expression for $\mathbb{B}$, (8), with respect to the yaw, roll, and pitch angles, as follows:

$$\frac{\partial \mathbb{B}}{\partial \psi} = \begin{bmatrix}0 & 0 & 0\\ 0 & -\sin\psi & \cos\psi\\ 0 & -\cos\psi & -\sin\psi\end{bmatrix}\mathbb{A}_\phi\mathbb{A}_\theta, \tag{79}$$

$$\frac{\partial \mathbb{B}}{\partial \phi} =\ \mathbb{A}_\psi\begin{bmatrix}-\sin\phi & 0 & \cos\phi\\ 0 & 0 & 0\\ -\cos\phi & 0 & -\sin\phi\end{bmatrix}\mathbb{A}_\theta, \tag{80}$$

and

$$\frac{\partial \mathbb{B}}{\partial \theta} =\ \mathbb{A}_\psi\mathbb{A}_\phi\begin{bmatrix}-\sin\theta & -\cos\theta & 0\\ \cos\theta & -\sin\theta & 0\\ 0 & 0 & 0\end{bmatrix}. \tag{81}$$

The 6×6 observation covariance matrix $\mathbb{R}$ is specified as diagonal, a simplification which ignores any coupling between the vector components. The covariances are based on an estimated uncertainty of 0.1° for the horizon scanners and 0.06° for the sun sensors. The sun sensor uncertainties are assumed to be constant in angular terms, which means the vector component variances decrease as the components (S_x, S_y, and S_z) approach ±1. The matrix is specified as:

$$\mathbb{R}\ =\ \begin{bmatrix}R_{S_x} & 0 & 0 & 0 & 0 & 0\\ 0 & R_{S_y} & 0 & 0 & 0 & 0\\ 0 & 0 & R_{S_z} & 0 & 0 & 0\\ 0 & 0 & 0 & R_H & 0 & 0\\ 0 & 0 & 0 & 0 & R_H & 0\\ 0 & 0 & 0 & 0 & 0 & R_H\end{bmatrix}, \tag{82}$$

where R_{S_x}, R_{S_y}, and R_{S_z} are the variances in S_x, S_y, and S_z, respectively, and R_H is the variance in the horizon vector, based on the above-stated uncertainties.

The 3×3 state noise covariance matrix $\mathbb{Q}$ is also diagonal, and is based on the expected variance of the actual attitude from the simple dynamics model. It is expressed as:

$$\mathbb{Q}\ =\ \begin{bmatrix}q_\psi\Delta t & 0 & 0\\ 0 & q_\phi\Delta t & 0\\ 0 & 0 & q_\theta\Delta t\end{bmatrix}, \tag{83}$$

where q_ψ, q_ϕ, and q_θ are the estimated time variances in yaw, roll, and pitch, respectively, and Δt is the time between scan lines, i.e., 2/3 s for GAC data and 1/6 s for LAC and HRPT. The variances need to allow for all pitch motion, which is not modeled, and also for the deviation of roll and yaw from the model of the inertial spin axis. The values were all chosen, after some experimentation, to be $2.5 \times 10^{-9}\,\mathrm{s}^{-1}$.

The state transition matrix, $\mathbb{D}$, is based on the dynamics model of the inertial spin axis, i.e., constant pitch angle and orbital coupling between roll and yaw. This is specified using a small angle approximation as

$$\mathbb{D}\ =\ \begin{bmatrix}1 & -\omega_o\Delta t & 0\\ \omega_o\Delta t & 1 & 0\\ 0 & 0 & 1\end{bmatrix}, \tag{84}$$

4.2 Kalman Smoother Implementation

The Kalman filter, as described by Fallon (1978), uses only previous data to estimate the state. The SeaWiFS attitude determination processing can take advantage of the fact that, except at the ends of a scene, both past and future measurements are available. This is done by making two passes through the scene, forwards and backwards, and

then computing a weighted average of the results for each scan line—this process is known as Kalman smoothing.

The processing is initialized for a scene by setting the state vector, $\vec{X}$, to all zeroes and $\mathbb{P}$, the state covariance matrix, to an identity matrix. For each scan line, the processing is as follows.

1. The state transition matrix and state noise covariance matrix ($\mathbb{D}$ and $\mathbb{Q}$, respectively) are computed using (83) and (84) based on the time from the previous scan line, Δt.
2. The previous values of $\vec{X}$ and $\mathbb{P}$ are then propagated using (73) and (74).
3. Then, if valid observations of $\vec{Y}$ are available, the model observations, partial derivatives, and observation covariance matrix ($\vec{G}$, $\mathbb{G}$, and $\mathbb{R}$, respectively) are computed using (75) through (82).
4. The gain matrix $\mathbb{K}$ is computed using (71), and is used to update $\vec{X}$ and $\mathbb{P}$ using (70) and (72).
5. The values of $\vec{X}$ and $\mathbb{P}$ are saved for each line.

The second pass is performed using $\vec{X}$ and $\mathbb{P}$ from the last scan line for initialization. The computations are identical except that Δt is negative. At each line, the weighted average of $\vec{X}$ is computed using the values of $\mathbb{P}$ from both passes, and saved as the final set of spacecraft attitude angles for that scan line.

5. FINAL PROCESSING

The final steps in navigation processing are: processing the SeaWiFS instrument tilt telemetry to determine the tilt angle for each scan line; combining the orbit, attitude and tilt information to compute the instrument pointing information for each scan line; and generating the data to be stored in the level-1a output product. These steps are described in the following subsections.

5.1 Tilt Data Processing

The SeaWiFS instrument can be commanded to three tilt states: nadir (0°), aft (20°), and forward (−20°). As stated in Sect. 1, the tilt consists of a rotation about the SeaWiFS z-axis. The standard operating scenario is to tilt aft for the first half of the data collection period in the orbit (i.e., north of the subsolar point) and forward for the second half. Other scenarios, primarily involving nadir tilt for part of an orbit, have been used on occasion. The tilt change takes about 13 s to complete.

The tilt telemetry consists of digital status bits and analog tilt motor angles, which are provided for two out of every three scan lines. The three status bits indicate one of the four possible states: nadir, aft, forward, or changing. In the first three states, the tilt angle can be assumed to be a fixed, predetermined value. The tilt angles at the three positions were measured prelaunch and is given in Table 2 (note that nadir has been defined to be exactly zero). During the tilt change periods, the tilt motor telemetry is used to compute the tilt angle, as described below. The tilt telemetry are validated by checking for single scan-line tilt states (indicative of corrupted telemetry), out-of-limit values, and monotonic behavior during tilt states. The tilt angles are interpolated to the scan lines without tilt information for which the tilt telemetry were flagged.

Table 2. Nominal and actual tilt angles

Tilt State	*Nominal Angle*	*Actual Angle*
Nadir	0°	0.0°
Aft	20°	19.820°
Forward	−20°	−19.925°

The tilt motor telemetry consists of angle measurements from two tilt motors, one mounted on the fixed base of the sensor and one on the tilting platform. The angles are referred to as Φ_B and Φ_P, respectively. After validation, the next step is to calibrate the angles and add an adjustment to the measurement reference points:

$$\Phi'_B \;=\; A_B\Phi_B \;+\; B_B \;+\; \Phi_{RB}, \tag{85}$$

and

$$\Phi'_P \;=\; A_P\Phi_P \;+\; B_P \;+\; \Phi_{RP}, \tag{86}$$

where Φ'_B and Φ'_P are the calibrated and adjusted motor angles; A_B and A_P are the calibration scale factors; B_B, and B_P are the biases; and Φ_{RB} and Φ_{RP} are the reference angle adjustments (80 and 235°, respectively).

The tilt mechanism includes the following fixed dimensions:

a) Pivot-to-base motor shaft, $d_B = 7.088$;
b) Pivot-to-platform motor shaft, $d_P = 6.000$;
c) Base-to-platform motor link, $d_l = 4.070$; and
d) Motor shaft-to-link radius, $d_r = 1.025$.

The tilt angle, Θ, is computed as follows:

$$\Theta \;= \Theta' \;-\; \Theta_B \;-\; \Theta_P \;-\; 35.068, \tag{87}$$

where

$$\Theta' \;=\; \cos^{-1}\left(\frac{{d'_B}^2 \;+\; {d'_P}^2 \;-\; d_l^2}{(2d'_B d'_P)}\right), \tag{88}$$

$$\Theta_B \;=\; \sin^{-1}\left(\frac{d_r \sin\Phi'_B}{d'_B}\right), \tag{89}$$

$$\Theta_P \;=\; \sin^{-1}\left(\frac{d_r \sin\Phi'_P}{d'_P}\right), \tag{90}$$

$$d'_B \;=\; \sqrt{d_B^2 \;+\; d_r^2 \;-\; 2d_B\, d_r \cos\Phi'_B}, \tag{91}$$

and

$$d'_P \;=\; \sqrt{d_P^2 \;+\; d_r^2 \;-\; 2d_P\, d_r \cos\Phi'_P}, \tag{92}$$

5.2 Final Attitude Processing

The data stored for each scan line consist of the orbit position vector, attitude angles, tilt angle, sun reference vector in the ECEF frame, sensor (ECEF-to-SeaWiFS) transformation matrix, and scan ellipse coefficients. In addition, flags are set if navigation cannot be computed for a scan line.

The computation of the orbit vector, attitude angles, tilt angle, and sun reference vector were described in previous sections. The sensor transformation matrix is computed by successively multiplying the ECEF-to-orbital, orbital-to-spacecraft, spacecraft-to-SeaWiFS, and tilt transformations:

$$\mathbb{M} = \mathbb{T}\mathbb{S}\mathbb{B}\mathbb{O}, \tag{93}$$

where the orbital-to-spacecraft transformation is computed using (8) and the yaw, roll, and pitch angles for the scan line.

The six scan ellipse coefficients are computed using the sensor transformation matrix and orbit position vector (Patt and Gregg 1994):

$$\begin{aligned} C_1 &= \mathbb{M}_{1,1}^2 + \mathbb{M}_{1,2}^2 + \frac{\mathbb{M}_{1,3}^2}{(1-f)^2} \\ &= 1 + \mathbb{M}_{1,3}^2 \left((1-f)^{-2} - 1\right), \end{aligned} \tag{94}$$

$$\begin{aligned} C_2 &= 2\mathbb{M}_{1,1}\mathbb{M}_{3,1} + 2\mathbb{M}_{1,2}\mathbb{M}_{3,2} + \frac{2\mathbb{M}_{1,3}\mathbb{M}_{3,3}}{(1-f)^2} \\ &= 2\mathbb{M}_{1,3}\mathbb{M}_{3,3} \left((1-f)^{-2} - 1\right), \end{aligned} \tag{95}$$

$$\begin{aligned} C_3 &= \mathbb{M}_{3,1}^2 + \mathbb{M}_{3,2}^2 + \frac{\mathbb{M}_{3,3}^2}{(1-f)^2} \\ &= 1 + \mathbb{M}_{3,3}^2 \left((1-f)^{-2} - 1\right), \end{aligned} \tag{96}$$

$$C_4 = 2\mathbb{M}_{1,1}P_x + 2\mathbb{M}_{1,2}P_y + \frac{2\mathbb{M}_{1,3}P_z}{(1-f)^2}, \tag{97}$$

$$C_5 = 2\mathbb{M}_{3,1}P_x + 2\mathbb{M}_{3,2}P_y + \frac{2\mathbb{M}_{3,3}P_z}{(1-f)^2}, \tag{98}$$

and

$$C_6 = P_x^2 + P_y^2 + \frac{P_z^2}{(1-f)^2} - R_E^2, \tag{99}$$

where $\mathbb{M}_{i,j}$ is the component of $\mathbb{M}$ in the ith row and jth column.

6. DISCUSSION

The navigation algorithms presented here are implemented in the operational data processing code and are used daily in the data processing performed by the SeaWiFS Project†. The accuracy of the navigation accuracy has been assessed continually through an automated method using island targets (Patt et al. 1997). This assessment has served to provide a public record of the accuracy of the current navigation processing‡, to indicate where the accuracy needs improvement, and to assess the effect of changes to the algorithms prior to their acceptance for operational processing.

Provided below is a brief summary of the accuracy assessed as various improvements to the processing were introduced since launch. It includes the typical accuracies now expected of the algorithms, and some cases that provide exceptions to the nominal performance are noted. In addition, brief observations are made on the potential for further improvements.

The changes to the algorithms since launch produced rapid improvements in accuracy early in the mission, and smaller improvements over longer time scales since then. Shortly after launch, the initial adjustments to the processing resulted in a typical 2σ accuracy of about 2 pixels, with considerable variation; the errors near the subsolar point were largely unknown. In early 1998, the attitude sensor alignments were refined, which reduced the typical accuracy to about 1.5 pixels, but the subsolar errors remained large.

During mid-1998, the Kalman smoother was implemented for attitude determination to replace the single-frame method, which was developed before launch. This was performed in anticipation of the single-ACS-string operation, which was planned to start later that year, and also to improve the subsolar accuracy. In this same time frame, the horizon angle model was modified to include a revised flattening factor and seasonal corrections. The combination of these improvements and additional refinement of the attitude sensor alignments produced typical accuracies of about 1.25 pixels, with subsolar errors of up to several pixels. These changes were incorporated for the reprocessing of the mission data in August and September 1998.

In 1999, analysis of the navigation assessment results for the entire mission indicated inconsistencies in the roll and yaw accuracies, with better results during the months of April–September at the expense of larger errors during October–March. This was traced to the use of a simplified form of the horizon scanner angle calibration, which was implemented shortly after launch. The calibration was modified to use look-up tables provided by the manufacturer. This improvement was used for the reprocessing in May 2000. With this change, the typical accuracies approached 1 pixel; errors of a few pixels were seen near, and just south of, the subsolar point, particularly during December–March.

Most recently, in early 2001, a further refinement to the horizon angle model was developed in response to navigation assessment results which indicated seasonal variations in the horizon flattening factor. A correction for this

† The SeaWiFS processing code is freely distributed by NASA to SeaWiFS data users and ground stations as part of the SeaWiFS Data Analysis System (SeaDAS).

‡ Available via the World Wide Web at the following URL: `http:\\algae2.gsfc.nasa.gov/navqc`.

was implemented, and the navigation accuracies since then have averaged 1 pixel or less, with maximum errors of less than 2 pixels. This change will be applied to the mission data set during the reprocessing in March or April 2002.

The *typical* accuracy is not achieved in a variety of special cases:

- *Time tag errors:* Occasional errors in the time tags for the science data have been discovered, which offset the geolocation in the along-track direction. Efforts are underway to correct or flag these occurrences during level-1a processing.
- *Polar horizon anomalies:* Winter polar stratospheric temperature variability affects the horizon scanner performance at high latitudes, degrading the roll accuracy.
- *Periods of high nutation:* High levels of nutation were triggered which occurred often in the early part of the mission, and occasionally thereafter. At these times, the tracking of the roll and yaw changes was less accurate.
- *Anomalous pitch motion:* Some fairly rapid pitch motions of the spacecraft have been caused by onboard GPS errors and from moon interference in the scanners; the current processing algorithms cannot always track these motions well.
- *Tilt change:* During the SeaWiFS instrument tilt change and for a few seconds before and after, the pitch accuracy is affected.
- *Short data spans:* For HRPT scenes less than about 5 min duration, especially in the subsolar region, accuracy is degraded.

Although further improvements are certainly possible, they would mainly reduce the maximum errors under certain unusual conditions as discussed above. The accuracy is currently pushed near the limits set by the performance of the attitude sensors and the fidelity of the spacecraft dynamics model. Further improvements would probably need to depend on modeling the spacecraft dynamics and onboard control responses, and this would present some challenges. Ultimately, this activity will continue according to the needs of the science-data users.

Glossary

ACS Attitude Control System
ASAP Artificial Satellite Analysis Program

COSMIC Computer Software Management and Information Center

DSS Digital Sun Sensor

ECEF Earth-Centered Earth-Fixed
ECI Earth-Centered Inertial
ECR Earth-Centered Rotating

FOV Field-Of-View

GAC Global Area Coverage
GPS Global Positioning System
GSFC Goddard Space Flight Center

HRPT High-Resolution Picture Transmission
HS Horizon Scanner

IQR Interquartile Range

LAC Local Area Coverage

NASA National Aeronautics and Space Administration

OV2 OrbView-2; satellite platform on which the SeaWiFS instrument is flown.

SeaDAS SeaWiFS Data Analysis System
SeaWiFS Sea-viewing Wide Field-of-view Sensor

URL Universal Resource Locator

Symbols

a Orbit semi-major axis.
A_B Tilt motor angle scale factor.
A_P Tilt motor angle scale factor.
A_α A DSS scale factor.
A_β A DSS scale factor.
$\mathbb{A}_\phi$ Roll angle rotation matrix.
$\mathbb{A}_\theta$ Pitch angle rotation matrix.
$\mathbb{A}_\psi$ Yaw angle rotation matrix.
$\mathbb{B}$ Orbital-to-spacecraft transformation matrix.
B_B Tilt motor angle bias.
B_P Tilt motor angle bias.
B_α DSS bias.
B_β DSS bias.
$\vec{c}_0$ Cubic polynomial coefficient vector.
$\vec{c}_1$ Cubic polynomial coefficient vector.
$\vec{c}_2$ Cubic polynomial coefficient vector.
$\vec{c}_3$ Cubic polynomial coefficient vector.
C_1 Scan ellipse coefficient.
C_2 Scan ellipse coefficient.
C_3 Scan ellipse coefficient.
C_4 Scan ellipse coefficient.
C_5 Scan ellipse coefficient.
C_6 Scan ellipse coefficient.
$\mathbb{C}$ DSS-to-spacecraft transformation matrix.
$\mathbb{D}$ Kalman filter state transition matrix.
d_B Tilt pivot to base motor shaft dimension.
d'_B Tilt pivot to base motor link dimension.
d_l Tilt base motor to platform motor link dimension.
d_P Tilt pivot to platform motor shaft dimension.
d'_P Tilt pivot to platform motor link dimension.
d_r Tilt motor shaft to link dimension.
e Orbit eccentricity.
$\vec{E}$ Nadir vector in spacecraft frame.
$\mathbb{E}$ ECI-to-ECEF transformation matrix.
$\vec{E}_R$ Reference nadir vector.
f Earth flattening factor.
f_P Effective flattening factor at spacecraft position.
$\vec{G}$ Observation model vector.
$\mathbb{G}$ Partial derivative matrix.
G_m Earth gravitational constant.

$\vec{H}$ Horizon vector in spacecraft frame.
$\mathbb{H}$ HS-to-spacecraft transformation matrix.
H_1 Horizon angle model coefficient.
H_2 Horizon angle model coefficient.
H_3 Horizon angle model coefficient.
H_4 Horizon angle model coefficient.
H_5 Horizon angle model coefficient.
H_6 Horizon angle model coefficient.
$\vec{H}_H$ Horizon vector in HS frame.
$\vec{H}_S$ Horizon vector in spacecraft frame.

i Orbit inclination.
$\mathbb{I}$ Identity matrix.

J Loss function.
J_2 Earth gravity field perturbation term.

$\mathbb{K}$ Kalman filter gain matrix.

l Orbit right ascension of ascending node.
$\vec{L}$ Orbit plane normal vector.
L_x x component with relation to $\vec{L}$.
L_y y component with relation to $\vec{L}$.
L_z z component with relation to $\vec{L}$.

m Orbit mean anomaly.
$\mathbb{M}$ ECEF-to-SeaWiFS frame transformation matrix.

n Mean motion.
$\vec{N}$ North vector at orbit position.

o Orbit angle measured from the ascending node.
$\mathbb{O}$ ECEF-to-orbital transformation matrix.
$\vec{O}_x$ Orbital frame axis.
$\vec{O}_y$ Orbital frame axis.
$\vec{O}_z$ Orbital frame axis.

$\vec{P}$ Orbit position vector.
$\vec{P}_1$ Position vector at time t_1.
$\vec{P}_2$ Position vector at time t_2.
$\mathbb{P}$ State covariance matrix.
P_x x component with relation to $\vec{P}$.
P_y y component with relation to $\vec{P}$.
P_z z component with relation to $\vec{P}$.

q_θ Pitch angle state noise covariance.
q_ϕ Roll angle state noise covariance.
q_ψ Yaw angle state noise covariance.
$\mathbb{Q}$ State noise covariance matrix.

$\mathbb{R}$ Kalman filter measurement covariance matrix.
R_E Earth equatorial radius.
R_H Horizon scanner measurement variance.
R_M Earth mean radius.
R_S Sun sensor measurement variance.

$\mathbb{S}$ Spacecraft-to-SeaWiFS transformation matrix.
$\vec{S}_D$ Sun vector in DSS frame.
$\vec{S}_E$ Sun reference vector in ECEF frame.
$\vec{S}_R$ Sun reference vector in spacecraft frame.
$\vec{S}_S$ Sun vector in spacecraft frame.
S_x x component with relation to $\vec{S}$.
S_y y component with relation to $\vec{S}$.
S_z z component with relation to $\vec{S}$.

t Relative sample time.
t_s Sample time.
t_0 Epoch time.
t_1 Time of first vector used for interpolation.
t_2 Time of second vector used for interpolation.
T Transpose (of a matrix).
$\mathbb{T}$ Tilt transformation matrix.

u_1 Intermediate coefficient used to calculate the nadir vector.
u_2 Intermediate coefficient used to calculate the nadir vector.
u_3 Intermediate coefficient used to calculate the nadir vector.
$\vec{U}_1$ Intermediate vector for nadir vector calculation.
$\vec{U}_2$ Intermediate vector for nadir vector calculation.
$\vec{U}_3$ Intermediate vector for nadir vector calculation.

$\vec{V}$ Orbit velocity vector.
$\vec{V}_1$ Velocity vector at time t_1.
$\vec{V}_2$ Velocity vector at time t_2.
$\vec{V}_C$ Orbit velocity vector in ECEF frame corrected for Earth rotation rate.
V_x x component with relation to $\vec{V}$.
V_y y component with relation to $\vec{V}$.
V_z z component with relation to $\vec{V}$.

w Orbit argument of perigee.
$\mathbb{W}$ State weighting matrix.

x Reference frame axis, or component of a vector in this frame.
$\vec{X}$ State vector.
$\vec{X}(t)$ State vector at time t.

y Reference frame axis, or component of a vector in this frame.
$\vec{Y}$ Observation vector (GPS orbit position or ACS sensor vector measurements).

z Reference frame axis, or component of a vector in this frame.
$\vec{Z}$ Geocentric North Pole vector.

α DSS output angle.
α' DSS calibrated output angle.

β DSS output angle.
β' DSS calibrated output angle.

γ HS half-cone angle.

δr Seasonal adjustment to the Earth's radius.
δz Seasonal ellipsoid shift along the Earth's pole.
Δt Time difference.
ΔX State update vector.
$\Delta\Psi$ Azimuth offset.

θ Spacecraft pitch angle.
Θ SeaWiFS tilt angle.
Θ' Intermediate component of tilt calculation from (88) to (90).
Θ_B Intermediate component of tilt calculation from (88) to (90).
Θ_P Intermediate component of tilt calculation from (88) to (90).

λ Subsatellite latitude.
λ_S Subsolar latitude.

σ Standard deviation.

ν Orbit true anomaly.

ξ Greenwich Hour Angle.

ϕ Spacecraft roll angle.
Φ_B Raw tilt motor angle.
Φ'_B Calibrated tilt motor angle.
Φ_I HS crossing angle (in-crossing).
Φ_O HS crossing angle (out-crossing).
Φ_P Raw tilt motor angle.

Φ'_P Calibrated tilt motor angle.
Φ_{RB} Tilt motor reference angle.
Φ_{RP} Tilt motor reference angle.
Φ_S HS phase angle output.
ρ Horizon angle to geocentric nadir.
ψ Spacecraft yaw angle.
Ψ Azimuth of the horizon crossing relative to local North.
Ψ_{HS} Azimuth of HS axis.
Ψ_O Azimuth of orbital y axis.
ω_E Earth rotation rate.
ω_O Orbit rotation rate.
Ω Horizon scanner Earth chord angle output.

References

Chen, L.C., and G.M. Lerner, 1978: "Sun sensor models." In: Wertz, J.R., *Spacecraft Attitude Determination and Control,* D. Reidel Publishing Company, Dordrecht, Holland, 224–227.

Fallon, L., 1978: "Recursive least-squares estimators and Kalman filters." In: Wertz, J.R., *Spacecraft Attitude Determination and Control,* D. Reidel Publishing Company, Dordrecht, Holland, 459–469.

——, and P.V. Rigterink, 1978: "Introduction to estimation theory." In: Wertz, J.R., *Spacecraft Attitude Determination and Control,* D. Reidel Publishing Company, Dordrecht, Holland, 447–451.

Kwok, J., 1987: *The Artificial Satellite Analysis Program,* Computer Software Management and Information Center, Athens, Georgia, 92 pp.

Liu, K., 1978: "Earth oblateness modeling." In: Wertz, J.R., *Spacecraft Attitude Determination and Control,* D. Reidel Publishing Company, Dordrecht, Holland, 98–102.

Patt, F.S., and W.W. Gregg, 1994: Exact closed-form geolocation algorithm for Earth survey sensors. *Inter. J. Remote Sens.,* **15,** 3,719–3,734.

——, R.H. Woodward, and W.W. Gregg, 1997: An automated method for navigation assessment for Earth survey sensors using island targets. *Inter. J. Remote Sens.,* **18,** 3,311–3,336.

——, and S. Bilanow, 2001: "Horizon scanner triggering height analysis for OrbView-2." Proc. 2001 Flight Mechanics Symp., *NASA Contractor Rept., 2001-209986,* NASA Goddard Space Flight Center, Greenbelt, Maryland, 559–573.

Wertz, J.R., 1978: Solar system constants (Appendix L). *Spacecraft Attitude Determination and Control,* D. Reidel Publishing Company, Dordrecht, Holland, 819.

The SeaWiFS Postlaunch Technical Report Series

Vol. 1

Johnson, B.C., J.B. Fowler, and C.L. Cromer, 1998: The SeaWiFS Transfer Radiometer (SXR). *NASA Tech. Memo. 1998–206892, Vol. 1,* S.B. Hooker and E.R. Firestone, Eds., NASA Goddard Space Flight Center, Greenbelt, Maryland, 58 pp.

Vol. 2

Aiken, J., D.G. Cummings, S.W. Gibb, N.W. Rees, R. Woodd-Walker, E.M.S. Woodward, J. Woolfenden, S.B. Hooker, J-F. Berthon, C.D. Dempsey, D.J. Suggett, P. Wood, C. Donlon, N. González-Benítez, I. Huskin, M. Quevedo, R. Barciela-Fernandez, C. de Vargas, and C. McKee, 1998: AMT-5 Cruise Report. *NASA Tech. Memo. 1998–206892, Vol. 2,* S.B. Hooker and E.R. Firestone, Eds., NASA Goddard Space Flight Center, Greenbelt, Maryland, 113 pp.

Vol. 3

Hooker, S.B., G. Zibordi, G. Lazin, and S. McLean, 1999: The SeaBOARR-98 Field Campaign. *NASA Tech. Memo. 1999–206892, Vol. 3,* S.B. Hooker and E.R. Firestone, Eds., NASA Goddard Space Flight Center, Greenbelt, Maryland, 40 pp.

Vol. 4

Johnson, B.C., E.A. Early, R.E. Eplee, Jr., R.A. Barnes, and R.T. Caffrey, 1999: The 1997 Prelaunch Radiometric Calibration of SeaWiFS. *NASA Tech. Memo. 1999–206892, Vol. 4,* S.B. Hooker and E.R. Firestone, Eds., NASA Goddard Space Flight Center, Greenbelt, Maryland, 51 pp.

Vol. 5

Barnes, R.A., R.E. Eplee, Jr., S.F. Biggar, K.J. Thome, E.F. Zalewski, P.N. Slater, and A.W. Holmes 1999: The SeaWiFS Solar Radiation-Based Calibration and the Transfer-to-Orbit Experiment. *NASA Tech. Memo. 1999–206892, Vol. 5,* S.B. Hooker and E.R. Firestone, Eds., NASA Goddard Space Flight Center, 28 pp.

Vol. 6

Firestone, E.R., and S.B. Hooker, 2000: SeaWiFS Postlaunch Technical Report Series Cumulative Index: Volumes 1–5. *NASA Tech. Memo. 2000–206892, Vol. 6,* S.B. Hooker and E.R. Firestone, Eds., NASA Goddard Space Flight Center, Greenbelt, Maryland, 14 pp.

Vol. 7

Johnson, B.C., H.W. Yoon, S.S. Bruce, P-S. Shaw, A. Thompson, S.B. Hooker, R.E. Eplee, Jr., R.A. Barnes, S. Maritorena, and J.L. Mueller, 1999: The Fifth SeaWiFS Intercalibration Round-Robin Experiment (SIRREX-5), July 1996. *NASA Tech. Memo. 1999–206892, Vol. 7,* S.B. Hooker and E.R. Firestone, Eds., NASA Goddard Space Flight Center, 75 pp.

Vol. 8

Hooker, S.B., and G. Lazin, 2000: The SeaBOARR-99 Field Campaign. *NASA Tech. Memo. 2000–206892, Vol. 8,* S.B. Hooker and E.R. Firestone, Eds., NASA Goddard Space Flight Center, 46 pp.

Vol. 9

McClain, C.R., E.J. Ainsworth, R.A. Barnes, R.E. Eplee, Jr., F.S. Patt, W.D. Robinson, M. Wang, and S.W. Bailey, 2000: SeaWiFS Postlaunch Calibration and Validation Analyses, Part 1. *NASA Tech. Memo. 2000–206892, Vol. 9,* S.B. Hooker and E.R. Firestone, Eds., NASA Goddard Space Flight Center, 82 pp.

Vol. 10

McClain, C.R., R.A. Barnes, R.E. Eplee, Jr., B.A. Franz, N.C. Hsu, F.S. Patt, C.M. Pietras, W.D. Robinson, B.D. Schieber, G.M. Schmidt, M. Wang, S.W. Bailey, and P.J. Werdell, 2000: SeaWiFS Postlaunch Calibration and Validation Analyses, Part 2. *NASA Tech. Memo. 2000–206892, Vol. 10,* S.B. Hooker and E.R. Firestone, Eds., NASA Goddard Space Flight Center, 57 pp.

Vol. 11

O'Reilly, J.E., S. Maritorena, M.C. O'Brien, D.A. Siegel, D. Toole, D. Menzies, R.C. Smith, J.L. Mueller, B.G. Mitchell, M. Kahru, F.P. Chavez, G.F. Cota, S.B. Hooker, C.R. McClain, K.L. Carder, F. Müller-Karger, L. Harding, A. Magnuson, D. Phinney, G.F. Moore, J. Aiken, K.R. Arrigo, R. Letelier, and M. Culver 2000: SeaWiFS Postlaunch Calibration and Validation Analyses, Part 3. *NASA Tech. Memo. 2000–206892, Vol. 11,* S.B. Hooker and E.R. Firestone, Eds., NASA Goddard Space Flight Center, 49 pp.

Vol. 12

Firestone, E.R., and S.B. Hooker, 2000: SeaWiFS Postlaunch Technical Report Series Cumulative Index: Volumes 1–11. *NASA Tech. Memo. 2000–206892, Vol. 12,* S.B. Hooker and E.R. Firestone, Eds., NASA Goddard Space Flight Center, Greenbelt, Maryland, 24 pp.

Vol. 13

Hooker, S.B., G. Zibordi, J-F. Berthon, S.W. Bailey, and C.M. Pietras, 2000: The SeaWiFS Photometer Revision for Incident Surface Measurement (SeaPRISM) Field Commissioning. *NASA Tech. Memo. 2000–206892, Vol. 13,* S.B. Hooker and E.R. Firestone, Eds., NASA Goddard Space Flight Center, Greenbelt, Maryland, 24 pp.

Vol. 14

Hooker, S.B., H. Claustre, J. Ras, L. Van Heukelem, J-F. Berthon, C. Targa, D. van der Linde, R. Barlow, and H. Sessions, 2000: The First SeaWiFS HPLC Analysis Round-Robin Experiment (SeaHARRE-1). *NASA Tech. Memo. 2000–206892, Vol. 14,* S.B. Hooker and E.R. Firestone, Eds., NASA Goddard Space Flight Center, Greenbelt, Maryland, 42 pp.

Vol. 15

Hooker, S.B., G. Zibordi, J-F. Berthon, D. D'Alimonte, S. Maritorena, S. McLean, and J. Sildam, 2001: Results of the Second SeaWiFS Data Analysis Round Robin, March 2000 (DARR-00). *NASA Tech. Memo. 2001–206892, Vol. 15,* S.B. Hooker and E.R. Firestone, Eds., NASA Goddard Space Flight Center, Greenbelt, Maryland, 71 pp.

Vol. 16

Patt, F.S., 2002: Navigation Algorithms for the SeaWiFS Mission. *NASA Tech. Memo. 2002–206892, Vol. 16,* S.B. Hooker and E.R. Firestone, Eds., NASA Goddard Space Flight Center, Greenbelt, Maryland, 17 pp.